



Numerical investigation on the operation and energy demand of a seven-stage metal hydride hydrogen compression system for Hydrogen Refuelling Stations

Evangelos I. Gkanas^{a, c, *}, Christodoulos N. Christodoulou^{b, d}, George Tzamalīs^{b, c},
Emmanuel Stamatakis^c, Alexander Chronēos^a, Konstantinos Deligiannis^{b, c},
George Karagiorgis^b, Athanasios K. Stubos^c

^a Hydrogen for Mobility Lab, Materials and Processes for Energy Needs Research Group, Institute for Future Transport and Cities, Coventry University, Priory Street, Coventry, CV1 5FB, United Kingdom

^b HYSTORE Technologies Ltd, RES&H2 Department, 30 Spyrou Kyprianou, Ergates Industrial Area, Nicosia, 2643, Cyprus

^c National Centre for Scientific Research Demokritos, 15341, Agia Paraskevi, Attica, Greece

^d Frederick University, 7 Y. Frederickou Str., Pallouriotissa, 1036 Nicosia, Cyprus

ARTICLE INFO

Article history:

Received 7 November 2018

Received in revised form

16 July 2019

Accepted 21 August 2019

Available online 22 August 2019

Keywords:

Metal hydride hydrogen compressor

Multi-stage compression

Hydrogen storage

Metal hydrides

Numerical analysis

ABSTRACT

In the present work, a numerical analysis on the performance of a seven-stage metal hydride hydrogen compression (MHHC) system is introduced, presented and discussed. The operation efficiency and cost along with the reliability of hydrogen compression is of great importance for the future commercial availability of Hydrogen Refuelling Stations (HRS); thus, significant improvements in hydrogen compression must be achieved and novel methods and approaches are being investigated in that respect. MHHC's offer distinct advantages over conventional mechanical compressors and the present paper aims at contributing to the efficient design and upscaling of such device via advanced numerical simulations of a seven-stage MHHC. The numerical model was supported by and validated with solid experimental data. Furthermore, several different operational temperature ranges for the compressor were examined and the importance of the proper operation conditions is discussed in terms of temperature evolution, pressure profile, cycle duration, compression ratio, thermal energy demand and efficiency.

© 2019 Published by Elsevier Ltd.

1. Introduction

Over the past 5 years, there has been a significant reduction in the price of Fuel Cell Electric Vehicles (FCEVs) from more than \$ 100,000 to almost half (\$ 55,000) [1]. In addition, all the major Original Equipment Manufacturers (OEMs), such as Toyota, Hyundai, Daimler, Vauxhall and Nissan have plans to reduce the cost and increase the efficiency in order to fully commercialise the FCEVs by 2025 [2]. More specifically, Toyota aims to improve the driving range of the next Mirai to 700–750 km (435–466 miles) from the current range of 500 km (310 miles) and hit the target of 1000 km (620 miles) by 2025 [2]. The main obstacle for the full

implementation of the FCEVs in the market is the lack of hydrogen refuelling infrastructure [3,4]. It is believed that the development of hydrogen infrastructure should go in parallel with the efforts to commercialise and reduce the price of the FCEVs [5]. Today, there are more than 320 Hydrogen Refuelling Stations (HRSs) in operation with more than 2/3 to be publicly accessible [6]. A HRS typically requires the following components: Hydrogen production and purification, hydrogen compressor, hydrogen storage, safety and hydrogen dispenser [7]. The main hydrogen compression component used within the HRSs is the conventional mechanical compressors, such as diaphragm and/or reciprocating compressors [8]. It has been reported that from a techno-economic point of view, up to 40% of the total cost of a HRS arises from the compression system [9,10]. The concept of the utilisation of metal hydrides, which can store and release hydrogen via chemisorption under a heat-driven reaction, connected in series to compress hydrogen is not new. It has been introduced almost 40 years ago [11–13]. The technology of

* Corresponding author. Hydrogen for Mobility Lab, Materials and Processes for Energy Needs Research Group, Institute for Future Transport and Cities, Coventry University, Priory Street, Coventry, CV1 5FB, United Kingdom.

E-mail addresses: ac1029@coventry.ac.uk, egkanas@gmail.com (E.I. Gkanas).

metal hydride hydrogen compression (MHHC) offers a dynamic alternative to the conventional compressors, as well as to other competitive technologies such as electrochemical compression. The advantages of the MHHCs over the competitive technologies are the simplicity of operation, the absence of moving parts; hence minimise the cost for maintenance and technical support, silent operation, reliability and compactness [14–16]. In addition, out of the technical point of view, is important to note that the efficiency of the MHHCs can be drastically improved if solar energy and waste heat from industrial sources will utilised instead of electricity [17–20]. Despite the advantages of the MHHC's over the mechanical compressors, there is still room for further development. In a recent review study, Lototsky et al. [21] highlighted the necessity for the proper material selection to build a MHHC, either as a single stage device, or for multi-stage operation. Some of the most important requirements that those materials should fulfil are: The Pressure-composition-Temperature (P-C-T) properties between the compression stages to be tuneable to achieve the required compression ratio under the proper temperature ranges, the reversible storage capacity should be as high as possible, to minimise the amount of the material needed with fast kinetics; thus the compressor will operate on a fast cycle pace. The hysteresis and plateau slope effects should be at low levels, whereas cyclic stability as well as tolerance to impurities are highly recommended. A more extensive analysis on the MHHC materials properties and characteristics is offered in the review article by Lototsky et al. [21]. During the last three decades, there has been a tremendous progress in the development of materials for solid-state hydrogen storage for both transportation and stationary applications. Regarding the materials for MHHC applications, special attention has been paid to four main categories of materials: The AB₅-type intermetallics, the AB₂-type intermetallics, the BCC solid solution alloys and the AB (TiFe)-type intermetallics. The AB₅-type intermetallics have been extensively studied, as they can store/release hydrogen under moderate temperature and pressure conditions [22]. The most common AB₅-type intermetallic is LaNi₅ which presents attractive thermodynamic properties and is easy to synthesise [23–25]. To change the thermodynamic stability of LaNi₅ and make it more convenient for MHHC applications, substitutions can take place either on the A part or the B part. The A part can be substituted with Cerium, that will lower the stability and will increase the dissociation pressure [26,27]. For industrial-scale manufacturing, the substitution of the A part with Mm (mischmetal) has been suggested and introduced [28,29]. The Ni-part has been partially substituted with Co, Al, M or Sn to increase the stability and decrease the hydrogen pressures [30–32]. However, those modifications can affect the plateau slope and hysteresis, but on the other hand have found to be beneficial for the life cycle and the degradation of the materials with cycling [33–35]. The AB₂-based intermetallics are eligible to cover a wider range of operational pressures; some researchers are calling these intermetallics as 'high pressure' materials. The alloys of technological importance crystallize as either hexagonal C14 (MgZn₂) and C32 (MgNi₂) or cubic, C15 (MgCu₂) Laves phases, and in a number of cases are allotropic [36]. In general, those alloys can store a relatively large amount of hydrogen (up to 2 wt%), such as ZrV₂H₆ and ZrCr₂H₄. However, the formed hydrides are too stable for practical applications [37]. An effective solution is the partial substitution of the A (Zr with Ti) part and/or B part (mainly Ni, Mn, Cr, V, Fe) to destabilise the hydride [26]. For the operation at higher hydrogen pressures, in order those materials to be applicable for MHHC purposes, the Ti/Zr ratio on the A-part and the Fe content at the B-part [21,38,39]. Another type of intermetallics that have the potential to be used as materials for MHHC purposes are the AB-type TiFe based intermetallics. Although, they present some drawbacks,

such as the presence of two plateaus on the PCT isotherms, difficulties during the activation process and their resistivity to impurities is limited [26,40]. Finally, the V-based BCC solid solution alloys, are a type of materials suitable for MHHC applications [41,42]. The Vanadium is able to form two hydrides VH_{1-x} and VH_{2-x} and the transition from the mono-to dihydride is able to store and release almost 1.8 wt% under ambient conditions [43]. By introducing a certain amount of Ti (≤ 17.5 at%) within the V-alloys can increase the plateau pressure [44,45].

The modern MHHCs are in general rather complex systems, which include and integrate metal hydride beds, piping system and valves, as well as the heating/cooling systems [46]. In addition, for multi-stage MHHCs the number of the stages together with the nature and the properties of each stage material are defining the compression ratio, the efficiency and the installation/operational cost of the MHHC [47]. For the first stage of the compression, where the compressor is connected to the hydrogen production device, such as an electrolyser [48], usually a 'conventional' AB₅-type intermetallic is used, such as LaNi₅ [49], although several modifications can be done in the stoichiometry in both the A and B parts with Ce, Mm and Al [50], thus the plateau pressure will be increased and the modified intermetallics can be used for the upcoming stages (higher pressure stages) [51–57]. For the higher-pressure stages, the Laves Phase AB₂-type intermetallics have been extensively used and studied, usually based on the Zr–Ti–Cr–Fe–V family [58–64].

HYSTORE Technologies Ltd. has developed and demonstrated a six-stage MHHC [18]. The target behind the development of such a complex and potentially expensive system is that the MHHC was able to operate between the temperature range of 10 °C (low temperature) and 80 °C (high temperature), making the system suitable for operation under flat-plate solar heating and cooling. The compressor showed stability during the operation with a compression ratio of 31.4. The compressor was tested also under various cooling temperatures, starting from 5 °C up to 17 °C and no negative effects on the compression performance were observed; indicating that a solar adsorption cooler can achieve the required cooling capacity. In general, HYSTORE aims for lower temperature levels than most of the literature reports, where the data reported from Refs. [65,66] are comparable. Table 1 presents some relative projects and outcomes reported in the literature the last 15 years. One of the future targets, is the extension of the MHHC to achieve an outlet pressure of more than 350–400 bar with the same heating and cooling temperatures.

In summary, the experimentation with the 7-stage MHHC version (and the simulations described in the manuscript) was performed with a view to optimize the MHHC device and eliminate at the end some of these stages (as it was actually done in the final prototype). Starting with 7 stages was decided based on the following:

Table 1
Reports and outcomes published in the literature from the last 15 years.

Report	No. stages	T _L – T _H (°C)	P _{in} – P _{del} (bar)
Egenics [66]	6	25–85	1–206
Lototsky et al. [67]	2	25–180	7–200
Popenciu et al. [68]	3	20–80	2–60
Kim et al. [69]	1	20–90	7–40
Li et al. [70]	2	25–150	40–740
Wang et al. [71]	2	25–150	30–700
Muthukumar et al. [72]	1	25–95	5–43
Laurencelle et al. [73]	3	25–80	1–206
Lototsky et al. [74]	2	25–130	10–200
Kelly and Girdwood [20]	1	25–130	140–410

- 1) The MHC should operate at a relatively low temperature range (10–80 °C)
- 2) More stages (seven) means, taking advantage of higher MH charging and discharging capacities and potentially, achieving higher compression flows.
- 3) By studying experimentally and computationally the 7-stage MHHC, it is easier to optimize the efficiency of the MHHC by eliminating in the final design a few of the stages.

As already mentioned, the modern MHHCs are complex systems. In addition, the manufacturing of a large compression system needs to take into account the materials for the beds, the connections and the heat management of the reactors. Thus; the need for the development of numerical models and studies that will be able to describe the processes taking place during the compression is of great importance.

The numerical description for the hydrogen uptake-release and at the same time the coupling between two reactors needs to consider several important parameters [75]. A detailed analysis on the heat and mass transfer phenomena inside the metal hydride beds is necessary to evaluate the temperature distribution during the reaction, hydrogen's diffusion within the host lattice and the pressure evolution. In the literature, there are reliable procedures for the numerical description and modelling of the storage/release of hydrogen to/from the metal hydrides, based on the coupled heat and mass transfer [76–82]. On the technical part, for the integration of the heat and mass transfer models for the numerical description of MHHCs, various empirical and semi-empirical approaches have been introduced [83,84], based on experimental data. For the integration of a combined MHHC model with the detailed analysis of heat and mass transfer process within the hydrides, a hybrid model describing the free volume of the reactor has been suggested for a two-stage compression system [85], which has found to be able to simulate industrial scale compressors containing a large number of metal hydride beds operating asynchronously. The unsteady heat and mass transfer characteristics during the coupling between the metal hydride beds on a multi-scale MHHC have been utilised, where the heat, mass and momentum conservation equations have been solved simultaneously for the development of a three-stage MHHC [86]. In addition, the influence of the operating parameters, such as the temperature of the heat source and sink, the operational pressure range and cycle time in a single stage MHHC have also been studied and evaluated [87]. In some other cases, the implementation of various H_2 equations of state in combination with realistic features in the hydrogen sorption properties were considered [88]. The study focused on evaluating the effect of the implementation of real/ideal gas models and the way that the equations of state can affect the P-c-T isotherms. In another study, a dynamic response during hydrogen discharge was introduced, where the factors that drive the hydrogen were taken into account; the pressure difference between the 'free' hydrogen and the atmosphere, as well as the actual desorption from the metal hydride [89]. In a previous work [90], the authors developed and presented a numerical approach to describe the operation of a three stage MHHC and made a conversation regarding the selection of the materials and the number of compression stages. When building and developing a MHHC, it is crucial to select the number of stages according to the application, the thermal and cost requirements and the customer needs.

In the current work, a numerical analysis of a seven-stage compression system is introduced, analysed and presented. The main purpose of the current work is to investigate and evaluate the operational features and performance of a multiple-stage compressor that has been developed by HYSTORE [18]. As the development of an up-scaled MHHC is a complex process and very

expensive, the current numerical study aims to understand and evaluate the performance of a seven-stage compressor in terms of compression ratio, cycle time, energy consumption and efficiency prior to the development of a final design for the MHHC. In addition, the amount of hydrogen compressed per cycle (which depends among others on the amount of metal hydrides used in the various stages) is a parameter of interest. The numerical approach is based on the introduction of the unsteady heat and mass transfer conservation equations for the coupled reactors. At the same time, realistic parameters were extracted for all the materials, such as the plateau pressure and the hysteresis and incorporated within the model. In addition, as the hydrogen pressure during the compression reaches high levels, the compressibility has been taken into account in the model, to achieve more precise results. Another novelty of the current work is the introduction of an expression for the heat transfer coefficient, by utilizing the heat produced/consumed and the average temperature of the tank walls and the metal hydride. Finally, the thermal conductivity of the materials was calculated by incorporating the Zehner, Bauer and Schlunder method and considering the Knudsen effect. The numerical model was validated against solid experimental results. The seven-stage compression system is examined in terms of temperature, pressure and hydrogenation/dehydrogenation capacity during the operation of the compressor. Particularly, the temperature ranges at which the compression system operates is an important factor with dominant role for the application of the MHHC since it may allow efficient operation of the device based on readily available renewable heat (e.g. solar thermal or industrial waste heat). The target of HYSTORE is to operate the compressor between 10 °C (low temperature) and 80 °C (high temperature). For the dehydrogenation, besides the target temperature (80 °C), a sensitivity analysis has been made against higher temperatures (90–100–105–110 and 120 °C), to compare the operation of the MHHC in terms of both cycle time and compression ratio as well as energy consumption and efficiency.

2. Model formulation and problem definition

2.1. Introduction to a seven-stage MHHC cycle

A simplified seven-stage MHHC is presented in Fig. 1. In summary, a complete compression cycle takes place via the following

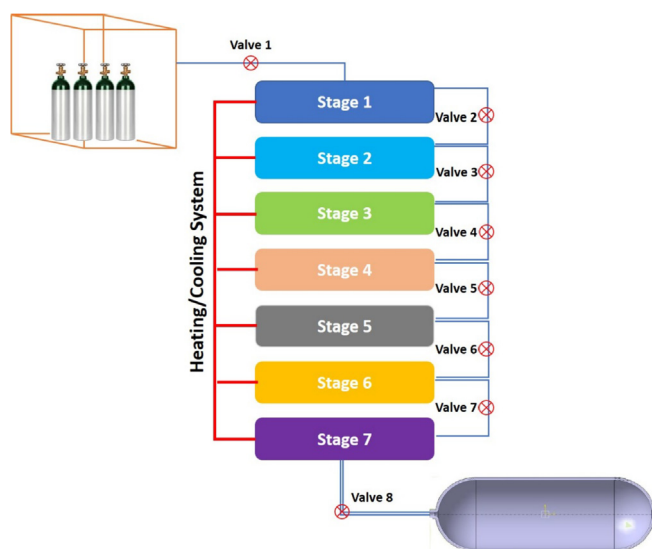


Fig. 1. Simplistic schematic of a seven-stage metal hydride hydrogen compressor.

steps:

- Step 1 Valve 1 (V1) opens and the low-pressure hydrogen supplier (electrolyser/hydrogen tank) is attached to the first stage tank. Hydrogen is stored during that step at a relatively low pressure. After the end of this process, Valve 1 closes and a sensible heating process begins.
- Step 2 A sensible heating of the first stage tank takes place at a predefined high temperature (T_H) to increase the pressure inside the tank and prepare the system for the next step. The sensible heating takes place every time before the coupling process (step 3 below) between the tanks.
- Step 3 Valve 2 opens between the first two hydride tanks. The temperature of the desorbing tank is high (T_H) and the temperature of the absorbing stage is low (T_L), thus, a coupling process between the two-stages occurs. The released hydrogen from the desorbing stage at a relatively high pressure is stored in the absorbing stage. This step is repeated for all seven tanks.
- Step 4 Valve 8 opens and the compressed hydrogen is released in the high-pressure storage tank, while reactor 1 is cooling down to be ready for the next compression cycle.

Fig. 2 illustrates the van't Hoff diagram based on the properties obtained from the actual materials. The dashed lines correspond to the dehydrogenation process and the solid lines to the hydrogenation process. After each storage process, a sensible heating of the tank occurs, to increase the equilibrium pressure; a necessary step to prepare the hydride for the upcoming dehydrogenation process at high pressure.

Furthermore, for a multi-stage compression system, the proper selection of the materials for each stage is a key factor that affects the effective and safe operation of the MHHC. The plateau (equilibrium) pressure for the hydrogenation of the first stage should be relatively low to allow the hydrogen storage from a low-pressure hydrogen supplier. One important aspect is that the equilibrium pressure for the dehydrogenation of every previous stage has to be

higher than the hydrogenation plateau pressure of each next stage during the coupling, so that the late tank will be able to store hydrogen at high pressure.

2.2. Mathematical model

To simplify the problem of hydrogen storage into the interstitial sites of the metal lattice, which is a complex process containing chemical reactions, diffusion and heat transfer phenomena, it is essential to make some assumptions for the establishment of the numerical model. The following assumptions have been considered for the current numerical approach.

- a) Initially the temperature and pressure profiles are uniform inside the tanks.
- b) The specific heat of the hydrides is assumed to be constant during the compression cycle.
- c) The medium is in local thermal equilibrium which implies that there is no heat transfer between solid and gas phases
- d) Radiative heat transfer and viscous dissipation are negligible.

2.2.1. Energy equation

Assuming thermal equilibrium between the hydride powder and hydrogen gas, a single energy equation is solved instead of two separate equations for both solid and gas phases, as the temperature of the gas and the solid as regarded as equal throughout the metal hydride tank:

$$(\rho \cdot Cp)_e \cdot \frac{\partial T}{\partial t} + (\rho_g \cdot Cp_g) \cdot \bar{v}_g \cdot \nabla T = \nabla \cdot (k_e \cdot \nabla T) + m \cdot (\Delta H - T \cdot (Cp_g - Cp_s) \times) \quad (1)$$

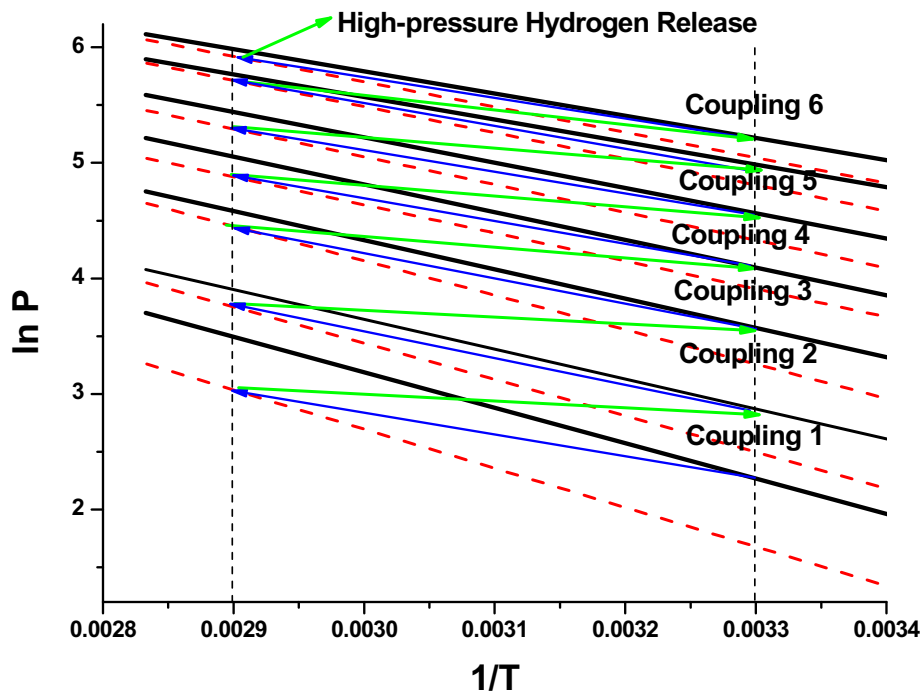


Fig. 2. van't Hoff diagram based on the properties of the actual materials used in the study for the operation steps of a seven-stage metal hydride hydrogen compressor.

Where m (kg/s/m^3) represents the kinetic term. Usually, the last term on the right hand is referred as *Heat Source* term (W/m^3). Eq (1) from the physical point of view, express the energy balance within porous media that contains a homogeneous mixture of species (hydrogen and the metal-hydride).

The effective heat capacity is given by:

$$(\rho \cdot Cp)_e = (\varepsilon \cdot \rho_g \cdot Cp_g) + ((1 - \varepsilon) \cdot \rho_s \cdot Cp_s) \quad (2)$$

For the introduction of the effective thermal conductivity, the Zehner, Bauer and Schlunder method, which is a model to predict the thermal conductivity within packed beds was used [91]. In the current work, the data from Ref. [92] were fitted to the following equation:

$$k_{eff} = \frac{C_1 \cdot p^{C_2}}{\frac{1}{C_0} + p^{C_2}} \quad (3)$$

Where, the C_0 , C_1 and C_2 are fitting coefficients [93].

2.2.2. Hydrogen and solid (metal/hydride) mass balance

The mass balance equation for hydrogen gas inside the tank is described from the continuity equation as follows:

$$\varepsilon \cdot \frac{\partial(\rho_g)}{\partial t} + \text{div}(\rho_g \cdot \vec{v}_g) = -m \quad (4)$$

While for the solid phase (metal/hydride) is given by the following:

$$(1 - \varepsilon) \cdot \frac{\partial \rho^{solid}}{\partial t} = m \quad (5)$$

The density of hydrogen is updated from the following expression:

$$\rho_g = \frac{p \cdot M_g}{Z(p, T) \cdot R \cdot T} \quad (6)$$

Where $z(p, T)$ is the compressibility factor, that represents the deviation of a real gas from the ideal behavior. For the needs of the current study, the compressibility factor was interpolated from the values taken from Ref. [94].

2.2.3. Momentum balance

The velocity of a gas passing through a porous medium can be expressed by Darcy's law. Darcy's law describes the flow of a fluid through a porous medium and by neglecting the gravitational effect, is a simple proportional relationship between the instantaneous flow rate through a porous medium with permeability K (m^2) and the pressure drop over a given distance and is given by:

$$\vec{v} = -\frac{k}{\mu} \cdot \nabla p \quad (7)$$

Where K (m^2) is the permeability of the solid and μ (m^2/s) is the dynamic viscosity of gas at the system working temperature. The pressure drop of gas, which is the driving force is the factor ∇p . The permeability for the solid state is given by the Kozeny–Carman's equation

$$K = \frac{dp^2 \cdot \varepsilon^3}{180 \cdot (1 - \varepsilon^2)} \quad (8)$$

Where dp is the mean particle diameter in the packed bed.

2.2.4. Reaction kinetics

In equations (1), (4) and (5), the m term represents the amount of hydrogen that is stored and released in the materials. The uptake and releasing rates in the current study are updated by the following expressions [95]:

For the hydrogenation process:

$$m_{abs} = C_{abs} \cdot \exp \left[-\frac{E_a}{R_g \cdot T} \right] \cdot \ln \left[\frac{p_g}{P_{eq}} \right] \cdot (\rho_{ss} - \rho_s) \quad (9)$$

For the dehydrogenation process:

$$m_{des} = C_{des} \cdot \exp \left[-\frac{E_d}{R_g \cdot T} \right] \cdot \left(\frac{P_{eq} - p_g}{P_{eq}} \right) \cdot \rho_s \quad (10)$$

Where C_a [s^{-1}] and C_d [s^{-1}] are pre-exponential constants for absorption and desorption respectively, E_a [J/mol] and E_d [J/mol] are the absorption/desorption activation energy, ρ_{ss} [kg/m^3] is the saturation density for hydride, and ρ_o [kg/m^3] is the initial metal hydride density.

2.2.5. Equilibrium pressure

Initially, the reactors are in equilibrium with the hydrogen gas. The hydride equilibrium pressure is estimated by using van't Hoff law [96]:

$$\ln P_{eq} = \left[\frac{\Delta H}{R_g \cdot T} - \frac{\Delta S}{R_g} + (\sigma_s \pm \sigma_0) \cdot \tan \left(\pi \left(\frac{X}{X_{max}} - \frac{1}{2} \right) \right) \pm \frac{Y}{2} \right] \cdot P_0 \quad (11)$$

Where σ_s and σ_0 are factors referring to the plateau slope flatness and Y is the hysteresis of the isotherm for the materials.

2.2.6. Coupled mass and energy balance

The hydrogen content and pressure of the system during the coupling between the desorbing and the absorbing stage after opening the valve is important and crucial for the compressor operation that needs to be considered when trying to describe the compression cycle. When the valve between the two coupled reactors opens, the reactor 1 is in direct contact with the interconnector, whereas the reactor 2 is also in direct contact with the interconnector; thus, the calculation of the hydrogen moles inside the interconnector with time is crucial, as it will play a dominant role during the coupling. The number of moles inside the interconnector between the two reactors is updated from the following equation:

$$n_t = n_{in} + n_{des} - n_{abs} \quad (12)$$

Where, n_{in} is the initial moles of hydrogen of the interconnector, n_{des} are the hydrogen moles that are entering the interconnector from the desorbing reaction (positive sign) and n_{abs} are the moles leaving the interconnector, as hydrogen is absorbed (negative sign).

Then, the pressure of hydrogen inside the interconnector is updated by:

$$p_t = \frac{n_t \cdot R_g \cdot T}{V_1 + V_2} \quad (13)$$

Where V_1 (m^3) and V_2 (m^3) are the free volumes of the reactor 1 and reactor 2 respectively and T (K) is the temperature of the gas inside the interconnector. Considering the pressure of hydrogen in the interconnector, we can use it as the driving force to drive hydrogen from the first stage to the second, therefore the kinetic equations for both hydrogenation and dehydrogenation process during the coupling are provided by the following equations.

$$m_{abs} = C_{abs} \cdot \exp\left(\frac{-E_a}{R_g \cdot T}\right) \cdot \ln\left(\frac{p_t}{P_{eq}}\right) \cdot (\rho_{ss} - \rho_s) \quad (14)$$

For hydrogenation and

$$m_{des} = C_{des} \cdot \exp\left(\frac{-E_d}{R_g \cdot T}\right) \cdot \left(\frac{P_{eq} - p_t}{P_{eq}}\right) \cdot (\rho_s) \quad (15)$$

For the dehydrogenation process.

3. Methodology

In the current numerical approach, the heat, mass and momentum conservation equations were solved simultaneously using a commercial Multiphysics package (COMSOL Multiphysics 5.3). The proposed numerical model was validated against experimental data for the hydrogen storage capacity and the temperature distribution during the hydrogen storage (exothermic)/release (endothermic). The expansion of the packed beds during the hydrogenation can introduce additional stresses to the vessel walls; therefore, the hydride beds are assumed to fill up to 50% with powder at the beginning of the hydrogenation. The expansion after the hydrogenation for all the materials was evaluated experimentally and was found to be between 28 and 33%. The seven different materials (one for each stage) were synthesized and tested to calculate the enthalpy and entropy change during the hydrogen uptake/release and to measure the hydrogen uptake/release capability. As mentioned earlier the main target is the operation of the MHHC between 10 °C–80 °C. Although, for comparison purposes and to get a clearer picture of the temperature effect during the compression, higher dehydrogenation temperatures were considered. The outcome of each simulation case was compared to that of the others in terms of compression ratio, compression cycle time, thermal energy needs and thermal efficiency per compression cycle. Table 2 summarizes the compression cases simulated in the current work.

3.1. Material selection

Seven different materials have been synthesized and tested regarding their thermodynamic and hydrogen uptake/release properties by HYSTORE Technologies Ltd. At the first stage, an AB₅-intermetallic (Mm-based) was utilised, while for the remaining six stages, AB₂-intermetallics (Zr–Ti–Mn–Co–Cr–Fe–V) were selected. All the above mentioned intermetallics were synthesized by arc-melting and characterized by means of XRD (BRUKER AXS D8-Advance Diffractometer) and SEM (Zeiss NEON 40 EsB Microscope), in order to identify the relevant microstructure while their P–c–T properties were measured by a commercial Sievert-type apparatus (Hidden Isochema), to estimate the thermodynamic properties needed for the numerical calculations. Table 3 presents the materials used for all the compression stages and some of their thermodynamic properties.

Table 2
Compression cases used in the current work.

Case	Hydrogenation Temperature (°C)	Dehydrogenation Temperature (°C)
Case 1	10	80
Case 2	10	90
Case 3	10	100
Case 4	10	105
Case 5	10	110
Case 6	10	120

3.2. Geometry of the system

The schematic of the metal hydride tanks used in the current study is shown in Fig. 3. The geometry of each tank is cylindrical, and each tank was filled up to 50%, to avoid any issues related to expansion of the metal hydride during the storage. The target of the study was the compression of 0.425 kgH₂ per compression cycle; thus, almost 31 kg of the AB₅-alloy was used for the first stage, while for the remaining stages, the amount of material was lower (almost 29.5 kg). The reason for that is the difference in the amount of hydrogen that the AB₅-alloy is able to store as compared to the AB₂-alloys and the difference in density. For that reason, the cylinders have the following dimensions: The length of each reactor is L = 12m and the heat management is achieved by the intermediate cylindrical shell, where the heating/cooling medium circulates. The radius of the internal cylinder that the metal hydride is placed is R = 21.4 mm. The external stainless-steel wall (SS 316L) thickness is 2 mm and the internal SS wall thickness is 8.75 mm. Finally, the thickness of the cylindrical shell of the heating/cooling fluid is 3.85 mm as presented in Fig. 3. For computational reasons, as the number of the domain elements exceeded 15,000,000, in order to reduce the computational time, the length of the reactors was considered as L = 6m. The porosity for porous materials in general is not constant during the hydrogen storage/release and is affected by the granular segmentation, densification and agglomerate growth within the metal hydride reactor. At the same time, the packing condition and the reactor shape also affect the porosity of the material. In the current work, the porosity for all the synthesized samples was measured experimentally by standard capillary porosimetry. The instrument used was the Pascal EVO 240 Porosimeter (Thermo Scientific) and the range of the porosity values for all the samples was found to be between 0.48 and 0.59. Especially for the materials S5, S6 and S7 (Table 3) the porosity measurements were very close to each other (almost 0.56). Thus, for simplicity in the calculations of the effective density, the effective heat capacity and thermal conductivity, the porosity of all the materials was chosen as 0.5 (i.e. the void volume inside the material is taken to be 50%). At the centre of the tank, a hydrogen supply porous sintered filter is placed which delivers hydrogen during the hydrogenation process and removes the released hydrogen during the dehydrogenation process.

3.3. Validation of the proposed numerical model

Properties such as density and thermal conductivity of both the bulk materials and the powders were measured for all the samples of the metal hydride materials. Coarse samples of the alloys were crashed into fine powder via sensitive ball milling. The density was measured in a gas displacement pycnometry system (Micrometrics Accupycn1340). The thermal conductivities of the samples were measured using a TCI Thermal Conductivity Analyzer (C-therm Technologies). Samples from the ball milled alloys were placed within a commercial Sievert-type apparatus (Hidden Isochema). Initially, the sample was degassed under high vacuum and the P–c–T isotherms were obtained at several temperatures (at least three) under the same ratio of the supply pressure to the equilibrium pressure, in order to plot the van't Hoff diagram. From the van't Hoff diagrams the reaction enthalpy and entropy changes were obtained. For the validation of the proposed numerical model, a comparison between experimental data with the results extracted from the numerical model has been considered. The experimental data were collected using a commercial Sievert-type apparatus (Hidden Isochema). An amount of 0.85 g of the AB₂-alloy that in the current study will be used for the second stage of the compression was used. A K-type thermocouple was placed inside the tank for the

Table 3

Materials used for each stage of the compressor and their thermodynamic properties.

Material	Type	ΔH (abs) J/molH ₂	ΔS (abs) J/molH ₂ K	ΔH (des) J/molH ₂	ΔS (des) J/molH ₂ K
S1	AB ₅	25242	104.6	28195	106.8
S2	AB ₂	21466	94.7	26133	107.1
S3	AB ₂	20354	101.1	24823	108.7
S4	AB ₂	19991	100.2	20252	100.8
S5	AB ₂	18198	98.12	19856	101.4
S6	AB ₂	16232	98.05	19125	101.5
S7	AB ₂	14702	98.1	18916	106.2

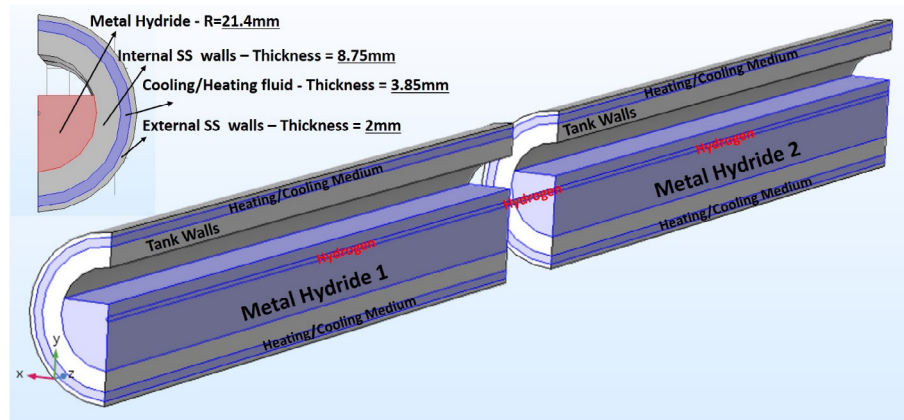


Fig. 3. Geometry of the reactors used in the current study. The reactors are of cylindrical shape with the length of each tube $L = 6$ m. The heating/cooling process is achieved by the intermediate cylindrical shell where the medium is placed.

measurement and recording of the hydride's temperature. Fig. 4 shows the temperature profile during the hydrogenation process (Fig. 4a) and the hydrogenation profile (Fig. 4b). The straight lines represent the simulation results and the dots represent the experimental data. It is observed that the numerically predicted temperature and hydrogenation behavior are in very good agreement with the experimental results.

4. Results and discussion

4.1. Temperature profile of the complete seven-stage compression cycle

In general, a multi-stage compression system based on the usage of metal hydrides utilizes several different materials with unique thermodynamic properties to increase the final compression ratio, while maximizing the hydrogenation rate from the supply pressure at each stage. The complete compression cycle for a seven-stage compressor consists of one independent hydrogenation process at the first stage with a subsequent sensible heating. The sensible heating is necessary for the increase of the equilibrium pressure for the upcoming dehydrogenation. Then, a coupling process (dehydrogenation-hydrogenation) takes place, where the hydrogen released from every previous stage is stored in the next stage. For the seven-stage compressor, there are six coupling processes, where after the end of every coupling, the sensible heating takes place. Finally, during the final dehydrogenation process, high pressure hydrogen is stored in a high-pressure storage tank. In the current work, several scenarios regarding the dehydrogenation temperature were investigated. The dehydrogenation temperatures studied were 80–90–100–105–110 and 120 °C. The temperature evolution of all the different stages for the complete compression cycle when the dehydrogenation process is 110 °C is presented in

Fig. 5.

During the first part of the hydrogenation, due to the exothermic nature of the reaction, a sudden increase of the hydride bed average temperature is observed. The temperature increase reaches a plateau (maximum) value and then gradually declines towards the temperature of the coolant. The temperature drop is not instantaneous, but a certain amount of time is necessary for the hydride to reach a lower temperature, as a result of the heat capacity of the reactors (tanks). This behavior can be explained thermodynamically and is due to the low thermal conductivity values that the hydride powders possess, which doesn't allow the generated amount of heat to be transferred with a sufficiently fast rate from the hydride to the coolant. In addition, due to the considerably high values of hydrogen pressure during compression, for safety reasons, the thickness of the internal SS wall is large, making the heat removal/supply less efficient. After the proper amount of hydrogen has been stored, the tank is heated up to a predefined temperature (in the case of Fig. 5 and 110 °C), to increase the equilibrium pressure and to accelerate the coupling process between the adjacent stage reactors. The dehydrogenation process is an endothermic reaction; thus, an amount of thermal energy must be provided to the hydride. During the initial stage of the dehydrogenation, the necessary amount of heat has not yet been effectively transferred from the heating fluid to the material, especially towards the material core, due to the poor thermal conductivity, resulting in a sudden temperature drop, as the hydride allows the hydrogen release by 'borrowing' an amount of thermal energy from the hydride itself. After the necessary amount of thermal energy from the external heating fluid reaches the bulk hydride, the temperature gradually starts to increase. As seen in Fig. 5, the maximum temperature that each hydride reaches during the hydrogenation process and/or the minimum temperature during dehydrogenation, depends on several parameters, such as the thermal conductivity,

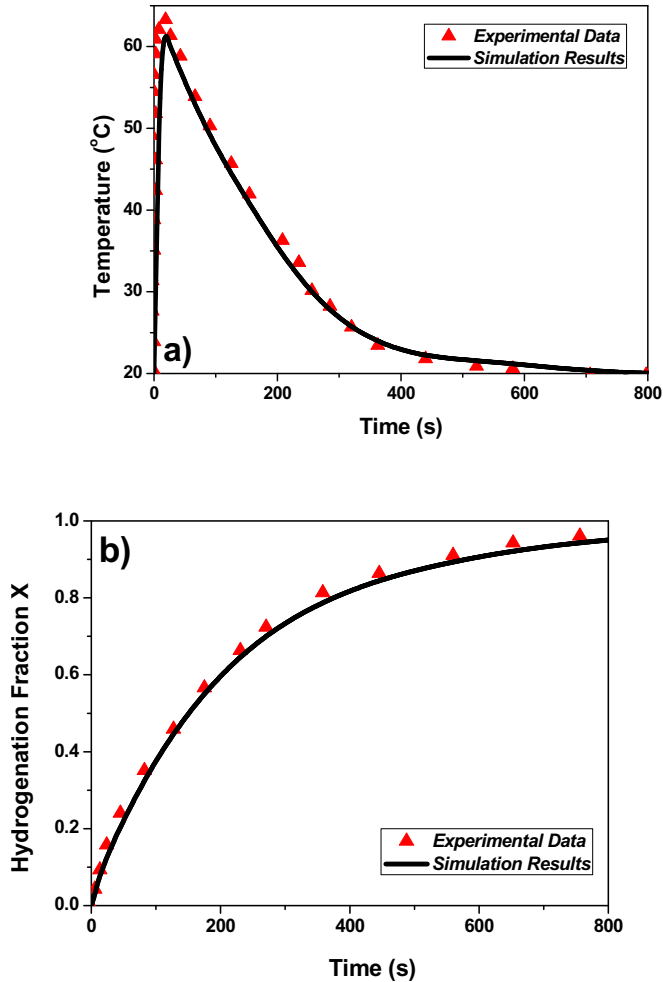


Fig. 4. Validation of the predicted temperature profile during the hydrogenation process with the actual temperature profile (Fig. 4a) and the hydrogen storage profile (Fig. 4b).

the specific heat capacity, the initial pressure and the effective density.

4.2. Pressure profile of the complete seven-stage compression system

Initially, a low-pressure hydrogen supplier (such as a commercial electrolyser, hydrogen cylinder, etc.) is attached to the first stage. The initial supply pressure chosen for this study is 20 bar. The initial temperature of the hydride is 10 °C; at that temperature the equilibrium pressure for the first stage hydride is 6.4 bar. When Valve 1 opens (Fig. 1) hydrogen flows from the hydrogen supplier to the first stage tank; the pressure difference is the driving force that allows hydrogen to be stored in the metal lattice. As expected, the hydrogen pressure during the hydrogen storage phase drops, as it is shown in Fig. 6 (First stage uptake).

After the hydrogenation reaches an equilibrium, a sensible heating of the tank takes place. During the heating process, an increase in the bed's pressure is expected as per van't Hoff law. After the hydride temperature has reached the desirable value (in this case 110 °C), the system is in the proper conditions for the first coupling process. The second stage tank, which is expected to store the released hydrogen from the previous stage is at a low initial temperature (10 °C). At that point, Valve 2 between the two

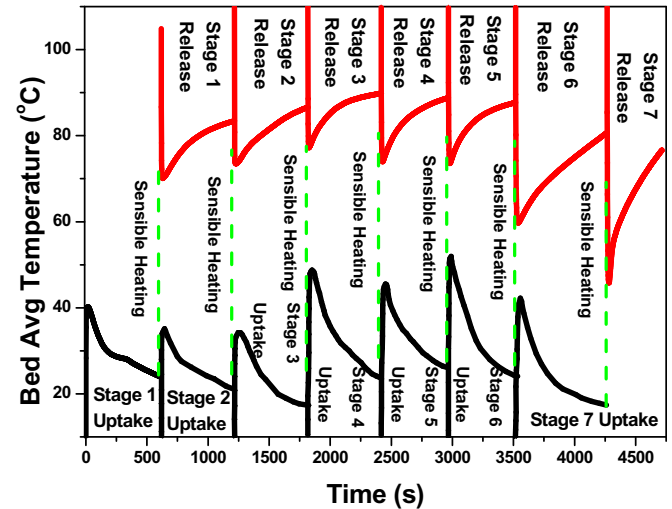


Fig. 5. Bed average temperature profile for the complete seven-stage cycle with time when the dehydrogenation temperature is 110 °C. The seven sensible heating processes are illustrated for simplicity with the vertical dashed lines.

reactors opens and the released hydrogen from the first stage flows towards the second reactor. The pressure difference between the two tanks is the driving force for the hydrogen flow from the releasing tank to the hydrogen storing tank, where hydrogen is now stored at higher pressure. During the initial phase of this coupling process, the equilibrium pressure of the releasing tank decreases while the equilibrium pressure of the hydrogenated tank increases sharply due to the very fast temperature kinetics between the two tanks. At some point in time, this coupling process reaches a maximum rate. Following this, the pressure of hydrogen inside both coupling reactors increases smoothly due to the presence of the driving potential. This process is depicted on the inset of Fig. 6. It has to be mentioned that for the operation of the current multi-stage compressor, during the coupling process the valve remains open between the tanks until the storing tank reaches 85–90% of its maximum storage capacity. The main reason for this decision, is that after the hydride stores around 85% of its maximum hydrogen capacity, the remaining amount of hydrogen is stored on a progressively slower rate, as the system reaches a plateau; thus, to keep the compressor operating, the valve between the reactors closes when the hydride reaches that plateau. The hydrogenation/dehydrogenation capacity for the complete compression cycle when the dehydrogenation temperature is 110 °C is presented in Fig. 7.

The operation of the compressor has been studied under various dehydrogenation temperatures (80–90–100–105–110 and 120 °C) and the comparison of the pressure profiles for all these different dehydrogenation temperatures is presented in Fig. 8.

As the dehydrogenation temperature increases, the duration of the coupling processes between the tanks becomes shorter and the pressure at the end of each successive coupling process reaches a higher value. The increase of the temperature directly affects the equilibrium pressure, as indicated by Eq. (11) and subsequently, the pressure difference between two adjacent tanks will increase. As this pressure difference is the driving force for the coupling process and the increase in the kinetics of the coupling depends on that difference, it is expected that the higher the pressure difference, the faster the coupling process. This situation is also described in the figure inset, where for the third coupling process, the pressure profile for all the different temperature cases is compared. By increasing the dehydrogenation temperature from 80 °C to 120 °C

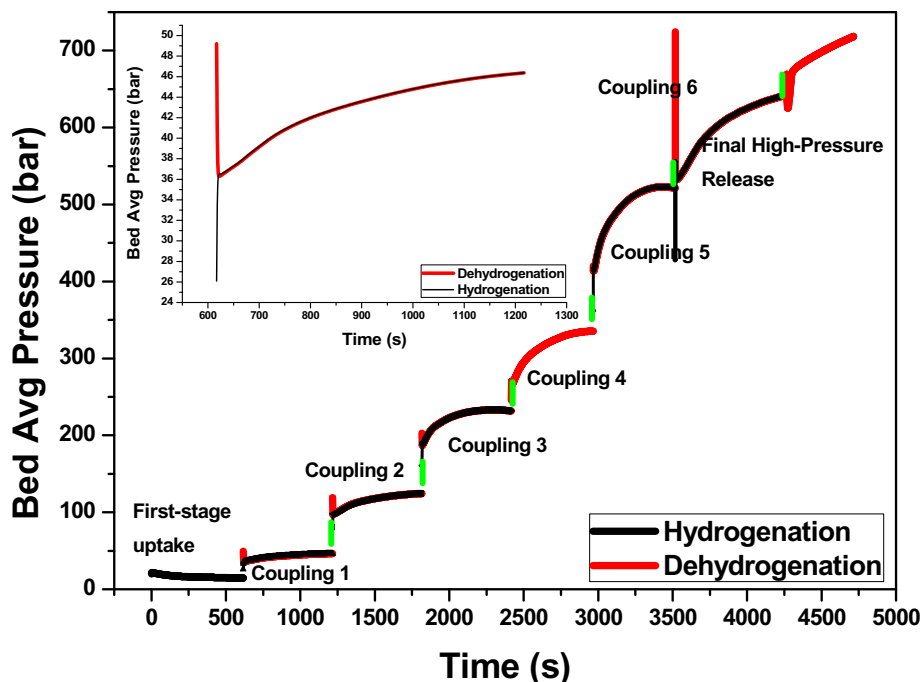


Fig. 6. Bed Average Pressure profile during a complete seven-stage compression cycle for the dehydrogenation temperature 110°C .

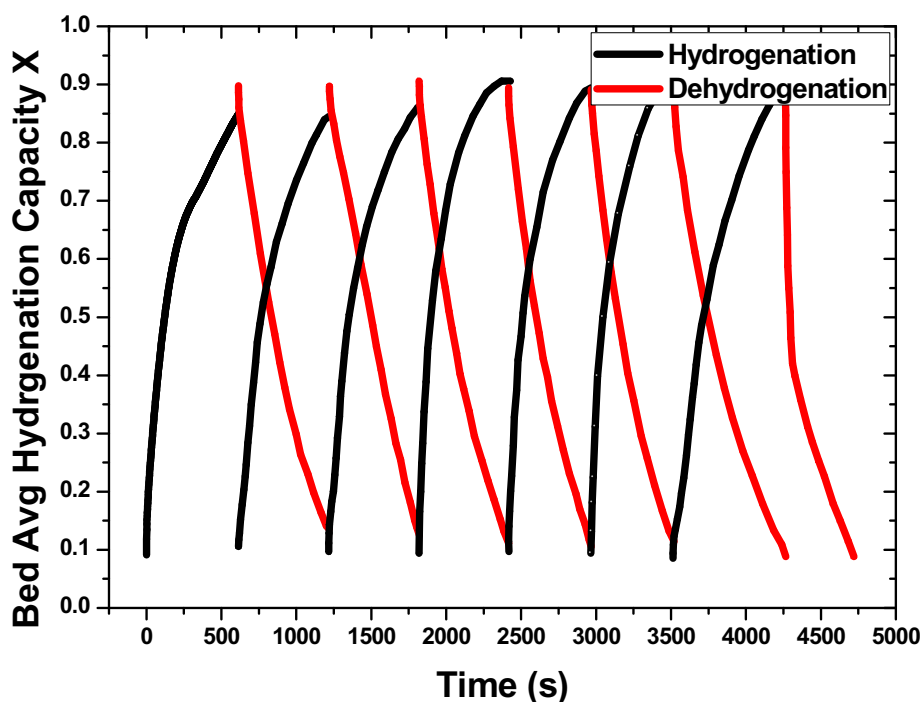


Fig. 7. Bed Average hydrogenation/dehydrogenation capacity for the complete compression cycle when the dehydrogenation temperature is 110°C .

the pressure can be increased from 180 bar (at 80°C) to 365 bar at (120°C). The summary of all the different complete compression cases is presented in 4.

For Case 1 ($10\text{--}80^{\circ}\text{C}$), a compression ratio of 18.7 is achieved at the end of the compression process. The complete cycle lasts slightly less than two hours (6625 s). The compression ratio increases with the dehydrogenation temperature and the cycle time drops, as the kinetics of the coupling are faster. For the case of

dehydrogenation temperature 100°C (Case 3), the time for a complete cycle is reduced by 40 min (1.41 h) while for the case of dehydrogenation temperature 120°C (Case 6) the cycle duration is slightly more than one hour.

4.3. Thermal energy demand for the complete compression cycle

The calculations for the thermal energy demand were utilised to

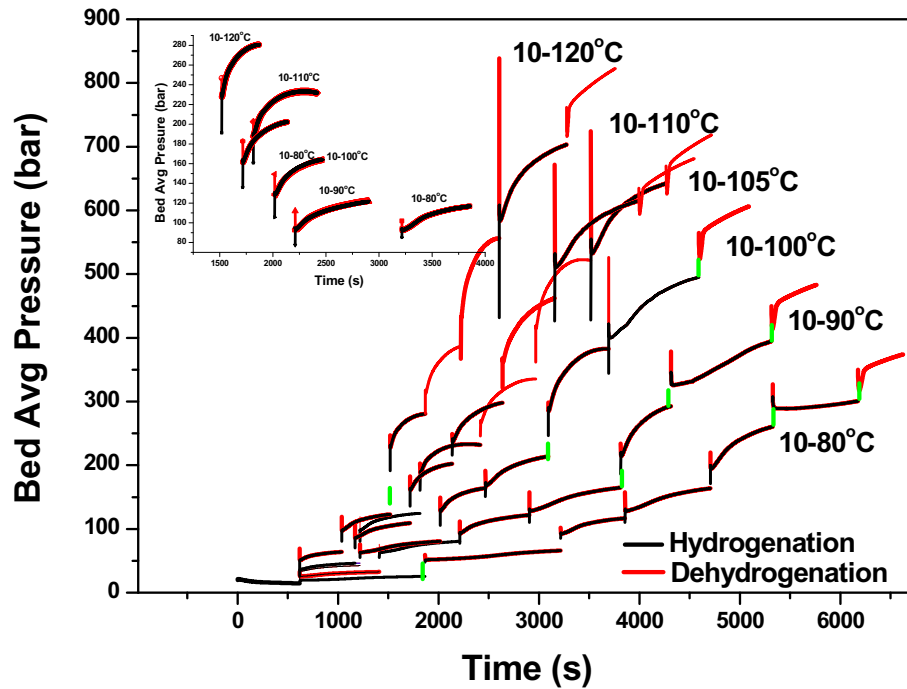


Fig. 8. Pressure profile for the complete compression cycle for all the different cases of dehydrogenation temperature (80-90-100-105-110 and 120 °C).

Table 4

Summary for the compression cases for all the studied temperatures.

Case	Initial Pressure (bar)	Final Pressure (bar)	Compression Ratio	Time (s)
Case 1	20	374	18.7	6625
Case 2	20	483.2	24.16	5760
Case 3	20	606.4	30.32	5090
Case 4	20	682	34.06	4720
Case 5	20	742	36.9	4530
Case 6	20	830	41.5	3760

extract some useful information regarding the thermal energy needs for the compressor operation. A MHHC is mainly based on a thermally-driven operation, where amounts of thermal energy are necessary to heat and to cool the metal hydrides. For each dehydrogenation process, there are two types of thermal energy to be supplied to the compressor; the first is the necessary amount of energy to heat the compressor, including the tank material (in this case is SS 316L) and the hydride material. The second type of energy is related to the necessary amount of energy to release the stored hydrogen from the alloy. The same process is required for the hydrogenation process. An amount of thermal energy is required to cool the reactor and the alloy powder, whereas an amount of energy is required to maintain the exothermic hydrogen storage. The energy for the compressor heating/cooling requires sensible heat that causes a temperature change ΔT , as well as latent heat, which will drive and maintain the dehydrogenation/hydrogenation reaction. Thus, the total amount of thermal energy is given from:

$$Q_t = Q_{sens} + Q_{lat} \quad (16)$$

Sensible heat is the thermal energy that has been exchanged between the thermodynamic system and its environment, that causes a temperature difference ΔT to the system. The sensible heating/cooling can be estimated by taking into account the mass of the system, the heat capacity and the temperature difference that is caused:

$$Q_{sens} = \sum_{i=1}^N (m_i \cdot C_i) \cdot \Delta T \quad (17)$$

Eq (17) represents the case where the sensible heating/cooling applies to several components. The term m_i (kg) represents the mass of each component, C_i (J/kg/K) is heat capacity of the component and ΔT (K) is the temperature difference. In the current case, there are two components that the sensible heating applies; the stainless-steel walls of tanks (SS 316L) and the alloy powder. The mass of the powder is 31 kg for stage 1 and 29.5 for the rest of the stages.

Regarding the SS 316L tank walls, the part of the cylinder to be heated/cooled is the cylindrical shell with $L = 12$ m, $R_{int} = 21.4$ mm and $R_{outer} = 30.15$ mm. The volume of the cylindrical shell is calculated from the following equation (18) and is equal to 0.017 m³

$$V = 2\pi \cdot r \cdot h \cdot \Delta r \quad (18)$$

Thus, the mass of the cylindrical shell to be heated/cooled is 136 kg. Based on these quantities, the total energy requirement in terms of sensible heating for the total compression cycle is presented on Table 5.

The latent heat that is necessary to remove/store hydrogen from the metal hydrides is equal to the heat of reaction as presented at Eq (1) and was calculated from the:

Table 5
Sensible thermal energy requirements for all the studied cases.

Case	Thermal Energy for SS 316L Walls (MJ)	Thermal Energy for Alloys Powder (MJ)	Total Sensible Thermal Energy Requirement (MJ)
1	63.31	8.45	71.76
2	72.35	9.66	82.02
3	81.41	10.87	92.27
4	85.92	11.47	97.39
5	90.44	12.08	102.52
6	99.48	13.28	112.77

$$Q_{lat} = \Delta H \cdot n_{H_2} \quad (19)$$

Where, n_{H_2} is the amount of hydrogen mole stored/released to/from the hydride.

Table 6 presents the thermal energy required to drive the reactions. In addition, the sensible thermal requirements are included along with the total thermal energy requirements and the compression ratio for all the studied cases. Finally, a small amount of heat is necessary to be provided to the desorbed amount of hydrogen (425 g) which also is present on Table 6.

As expected, while the temperature for the dehydrogenation process increases, the thermal energy demand reaches higher values. Furthermore, an attempt is made for a comparison between the values taken by the ratio: *Thermal Energy Demand/Compression Ratio* for the all the studied cases. For Case 1 (10–80 °C) the ratio takes the maximum value 2.03, while for all the remaining cases this ratio reduces gradually to 1.76–1.55 – 1.45–1.38 and 1.35. The profile of the thermal energy demand for the compressor, the compression ratio and the comparison ratio for all cases with the compression cycle time is presented in Fig. 9. For the later compression cycles, slightly lesser amounts of energy are required, as lesser amounts of hydrogen are compressed. Thus, the term $\Delta H \times n_{hydr}$ is lesser at every cycle. In addition, the thermal energy to heat the desorbed amount of hydrogen also is less.

4.4. Compressor efficiency

In essence, the MHHC is a heat engine that converts heat to work. In the case that the heat source and sink are utilised by renewables (solar thermal for the heat source and the atmosphere for the heat sink), the efficiency issue is not so important. Although, for the complete picture regarding the evaluation of the compressor's performance, in the current study the compressor efficiency has been calculated. To compare the MHHC compressor to the traditional mechanical piston-based compressors, the work required to achieve compression ratios of 18.7–24.16 – 30.32–34.06 – 36.9 and 41.5 was calculated. Four cases were introduced and compared. The first case is the isothermal compression, the second is the isentropic compression, whereas the last two are a polytropic approach and the isentropic by considering 75% efficient mechanical compressor (close to real life). A similar approach was reported from Ref. [20]. Table 7 presents the efficiencies for all the compression cases.

The efficiencies for the isothermal-isentropic and polytropic approaches was calculated from:

$$n_{th} = \frac{W}{Q} \cdot 100 \quad (20)$$

In the present work, the term Q is the amount of electrical energy to heat and cool the compressor by 70 °C (Case 1), 80 °C (Case 2), 90 °C (Case 3), 95 °C (Case 4), 100 °C (Case 5) and 110 °C (Case 6). The term n_c in the columns 3, 5, 7 and 9 is the 'second law efficiency', which is the ratio of the thermal efficiency to the Carnot efficiency:

$$n_c = \frac{n_{th}}{n_{carnot}} \quad (21)$$

The work for the isothermal compression was calculated from the equation:

$$W_{iso} = P_{low} \cdot V_l \cdot \ln r_p \quad (22)$$

Where P_{low} is the starting pressure, V_l is the specific volume of hydrogen at that pressure and r_p is the compression ratio. The isentropic work was calculated by the following equation:

$$W_s = \frac{k_p}{k_p - 1} \cdot P_{low} \cdot V_l \cdot \left(r_p^{\frac{k_p - 1}{k_p}} - 1 \right) \quad (23)$$

Where k_p is the ratio between the specific heat capacities under constant pressure to the specific heat capacity under constant volume. The polytropic work is updated from the following equation:

$$W_{pol} = \frac{n_p}{n_p - 1} \cdot P_{low} \cdot V_l \cdot \left(r_p^{\frac{n_p - 1}{n_p}} - 1 \right) \quad (24)$$

Where n_p is the polytropic coefficient. According to the outcomes presented in Table 7, the thermal efficiency varied from 2.4 to 4.51%, based on the compression scenario considered and the temperature range of the compression. According to the results, the thermal efficiency tends to drop when the dehydrogenation temperature

Table 6
Summary of the total heat thermal energy for a full compression cycle and the compression ratio.

Case	Total latent heat (MJ)	Total sensible heat (MJ)	Thermal Energy for Hydrogen (MJ)	Total thermal energy (MJ) – (kWh)	Compression Ratio
1	61.83	71.76	3.08	136.67–37.96	18.7
2	67.34	82.02	3.52	152.88–42.47	24.16
3	72.88	92.27	3.96	169.11–46.98	30.32
4	75.94	97.39	4.18	177.51–49.31	34.06
5	79.04	102.52	4.41	185.97–51.66	36.9
6	84.17	112.77	4.84	201.78–56.05	41.5

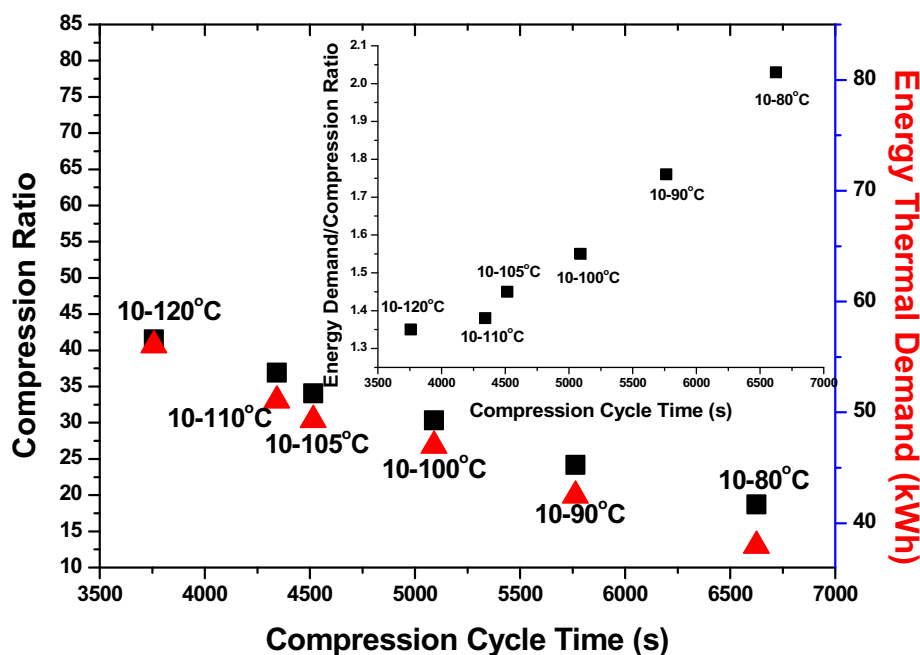


Fig. 9. Energy demand, compression ratio and comparison ratio over time for all the compression cases.

Table 7

Theoretical calculations for the compressor efficiencies.

Case	Isothermal Efficiency	Isothermal n_c	Isentropic Efficiency	Isentropic n_c	Polytropic Efficiency	Polytropic n_c	Adiabatic Irreversible	Isentropic Reversible n_c
1	2.78	14.05	4.39	22.16	3.98	20.01	3.29	16.62
2	2.71	12.28	4.45	19.99	3.99	17.93	3.34	14.99
3	2.62	10.87	4.48	18.59	3.98	16.5	3.36	13.94
4	2.58	10.28	4.51	17.93	3.99	15.88	3.38	13.45
5	2.52	9.66	4.46	17.08	3.93	15.01	3.34	12.81
6	2.4	8.58	4.33	15.47	3.81	13.59	3.25	11.60

increases. In addition, the 'second' law efficiency also drops as the desorption temperature increases, indicating that at lower dehydrogenation temperatures, although the compression ratio is less, the compressor efficiency is closer to the theoretical maximum efficiency (Carnot efficiency).

The operation of a MHHC is a thermally driven process; efficient heating and cooling of the compressor (hydride beds, hydrides and hydrogen) are necessary for the proper compression operation. There are several parameters and factors affecting the operation of a multi-stage compression system. The thermodynamic properties and the subsequent selection of the proper materials for the compression stages is a very important factor to increase the efficiency of a compressor. In addition, the operational temperature range is a very significant aspect that needs to be specified for the design of a MHHC. One of the outcomes of the current study is the impact and significance of the proper selection of the operational temperature conditions, with respect to the cycle duration (i.e. the hydrogen flowrate), the compression ratio, the thermal energy demand and the efficiency. It is important to understand and predict the performance of the compressor under different conditions and furthermore, to realise that the selection of the operational temperature range depends on the needs of the compressor end-user. If the main purpose is the quick delivery of high-pressure hydrogen and the cost of operation is of secondary importance, then the operation of the compressor at higher dehydrogenation temperatures (120 °C) is highly recommended. On the other hand,

if the primary scope for the compressor is the delivery of relatively high-pressure hydrogen at the lowest possible cost, by introducing renewables for the energy demand, then a relatively lower dehydrogenation temperature might be the preferable solution. In addition to that, the main scope of the current work was the study of a seven-stage MHHC that will operate within the temperature range 10–80 °C. The reason for the selection of this temperature range is the suitability of the system towards operation under solar heat and cooling. Another very important factor to increase the efficiency of the compressor is the development of a smart system for effective heat management to enhance the kinetics of the hydrogen storage/release processes. Contrary to the case of a heat management system for a conventional metal hydride tank that will be used only for hydrogen storage/release at a relatively low-pressure range and not for compression purposes, the heat management approach for the MHHC should be designed very carefully in terms of (among others) resistance to the large stresses due to the high-pressure range that will be applied during the compression. In conclusion, for the proper design of a compressor that will be based on metal hydrides, there are several factors that can affect the operation and the efficiency and should be considered. Thus, the design of an MHHC compressor should focus on the needs of the end-user and possibly sacrifice some characteristics in favor of some others depending on each individual case.

5. Conclusions

In this work, a numerical study describing the complete operation of a seven-stage MHHC is presented and analysed in terms of temperature distribution, pressure profile, compression ratio, thermal energy demand and thermal efficiency. The numerical model was validated against experimental data and very good agreement for both the temperature evolution and the hydrogenation profile was obtained. The main target of the overall work program is to develop a compressor that will be able to operate between the temperature range 10–80 °C and to utilise solar energy and/or waste heat for the operation of the compressor. In the current study, for comparison purposes, various temperature ranges were studied (80–90–100–105–110 and 120 °C). The main conclusions drawn from the current work are:

- As compared with the results from Ref. [64], the introduction of an extra stage has the capability to increase the final hydrogen pressure from 220 bar [64] to almost 365 bar. At the same time the introduction of an extra stage contributes to an extra energy addition of 4.8 kWh.
- The compression operation under the targeted temperature range presented a compression ratio of 18.7, total energy demand of 37.96 kWh, irreversible adiabatic efficiency 3.29% and second law irreversible adiabatic efficiency 16.62%. The increase of the dehydrogenation temperature to 120 °C instead of 80 °C resulted in a higher compression ratio (41.5), but at the same time to a higher thermal energy demand (56.05 kWh) with lower efficiencies (3.25% and 11.60%). In addition, for the dehydrogenation temperature 80 °C solar energy and waste heat can be utilised, whereas the higher operation temperatures may bring the complexity of using pumps and electricity for the operation.
- The MHHC is a technically viable alternative technology that is able to compress hydrogen to the required pressure for the refuelling of large-scale vehicles (buses, small trucks) as well as small scale vehicles (cars) if the energy needs are met by renewables and the hydrogen production is based on the use of renewable energy sources.
- The operation of a multi-stage metal hydride hydrogen compressor is affected by many parameters, among which the most important ones are: material thermodynamic properties, material storage/release kinetics, operation temperatures and heat management. Thus, several improvements are still needed before the commercialisation of MHHCs, from the development of more efficient materials, heat management techniques to automation and operation. For the design and development of a compression system based on metal hydrides, first the needs of the end-user should be defined, and the next step could be the analysis of the proper parameters that need to be taken into account for the development of the most efficient compression system. The present numerical study serves these purposes as it provides the model and tool for sensitivity analysis and optimization efforts.

Acknowledgments

The authors wish to acknowledge financial support by the European ATLAS-MHC project (PIAP-GA- 612292).

Nomenclature

C_a	Absorption Reaction Constant, s^{-1}
C_d	Desorption Reaction Constant, s^{-1}
C_p	Specific Heat, J/kg-K

E_a	Activation Energy for Absorption, J/molH ₂
E_d	Activation Energy for Desorption, J/molH ₂
h	Heat Transfer Coefficient, W/m ² K
k	Thermal Conductivity, W/m-K
K	Permeability, m ²
M	Molecular Weight, kg/mol
m	Kinetic Expression
n	Number of Hydrogen Moles
P	Pressure, bar
R	Gas Global Constant, J/mol-K
t	Time, s
T	Temperature, K
v	Gas Velocity, m/s
V	Volume, m ³
Q	Thermal Energy, J
m	mass, kg
C	Heat Capacity, J/kg/K
n_{th}	Thermal Efficiency
W	Compressor Work, J
r_p	Compression Ratio
k_p	Isentropic Ratio, C_p/C_v
n_p	Polytropic Coefficient

Subscripts

a	Absorption
A	Reactor A
B	Reactor B
d	Desorption
e	Effective
eq	Equilibrium
f	External Heater/Cooler
g	Gas
i	initial
s	Solid
ss	Saturation
th	Thermal
iso	Isothermal
S	Isentropic
pol	Polytropic

Greek Letters

ε	Porosity
μ	Dynamic Viscosity, kg/ms
ρ	Density, kg/m ³
ΔH	Reaction Enthalpy, J/mol
ΔS	Reaction Entropy, J/mol-K

References

- [1] Toyota Ushers in the Future with Launch of 'Mirai' Fuel Cell Sedan" (Press Release), Toyota Europe, Toyota City, Japan, 2014-11-01. Archived from the original on 2014-12-05. Retrieved 20/04/2019.
- [2] Retrieved 21/04/2019, <https://uk.reuters.com/article/us-toyota-hydrogen/toyota-plans-to-expand-production-shrink-cost-of-hydrogen-fuel-cell-vehicles-idUKKBN1KG0Y0>.
- [3] A. Mayyas, M. Mann, Manufacturing competitiveness analysis for hydrogen refueling stations, Int. J. Hydrogen Energy (2019), <https://doi.org/10.1016/j.ijhydene.2019.02.135>.
- [4] Y. Bicer, I. Dincer, Comparative life cycle assessment of hydrogen, methanol and electric vehicles from well to wheel, Int. J. Hydrogen Energy (2017), <https://doi.org/10.1016/j.ijhydene.2016.07.252>.
- [5] D. Apostolou, P. Enevoldsen, G. Xydis, Supporting green Urban mobility – the case of a small-scale autonomous hydrogen refuelling station, Int. J. Hydrogen Energy (2019), <https://doi.org/10.1016/j.ijhydene.2018.11.197>.
- [6] Wasserstoff-Tankstellen weltweit, Hydrogen Refuelling Stations Worldwide, H2-Stations, 2017. Available from: <https://www.netinform.de/H2/H2Stations/Default.aspx>. (Accessed 18 April 2019).
- [7] M. Iordache, D. Schitea, I. Iordache, Hydrogen refuelling station infrastructure roll-up, an indicative assessment of the commercial viability and profitability in the Member States of Europe Union, Int. J. Hydrogen Energy (2017), <https://doi.org/10.1016/j.ijhydene.2017.04.001>.

- doi.org/10.1016/j.ijhydene.2017.09.146.
- [8] E.I. Gkanas, M. Khzouz, Metal Hydride Hydrogen Compression Systems—Materials, Applications and Numerical Analysis, Hydrogen Storage Technologies. Sankir, M. & Sankir, N. D. (eds.), 1 ed. USA: Wiley, vol. 1, p. 3–37 35
 - [9] E. Stamatakis, E. Zoulas, G. Tzamalīs, Z. Massina, V. Analytis, C. Christodoulou, A. Stubos, Metal hydride hydrogen compressors: current developments and early markets, *Renew. Energy* (2018), <https://doi.org/10.1016/j.renene.2018.04.073>.
 - [10] C. Corgnale, M. Sulic, Techno-economic analysis of high-pressure metal hydride compression systems, *Metals* (Basel) (2018), <https://doi.org/10.3390/met8060469>.
 - [11] J.F. Lynch, A.J. Maeland, G.G. Libowitz, Hydrogen compression by metal hydrides, in: T.N. Veziroglu, I.B. Taylor (Eds.), *Hydrogen Energy Progress V. Proc. 5th World Hydrogen Energy Conference*, vol. 1, Pergamon Press, Oxford, 1984, pp. 1327–1337.
 - [12] P. Dantzer, E. Orgaz, Thermodynamics of the hydride chemical heat pump: model (I), *J. Chem. Phys.* 85 (1986) 2961–2973. <https://doi.org/10.1063/1.451006>.
 - [13] P. Dantzer, E. Orgaz, Thermodynamics of hydride chemical heat pump-II. How to select a pair of alloys, *Int. J. Hydrogen Energy* (1986), [https://doi.org/10.1016/0360-3199\(86\)90176-X](https://doi.org/10.1016/0360-3199(86)90176-X).
 - [14] K.B. Minko, M.S. Bocharnikov, Y.B. Yanenko, M.V. Lototsky, A. Kolesnikov, B.P. Tarasov, Numerical and experimental study of heat-and-mass transfer processes in two-stage metal hydride hydrogen compressor, *Int. J. Hydrogen Energy* (2018), <https://doi.org/10.1016/j.ijhydene.2018.09.211>.
 - [15] M. Lototsky, B. Satya Sekhar, P. Muthukumar, V. Linkov, B.G. Pollet, Niche applications of metal hydrides and related thermal management issues, *J. Alloy. Comp.* (2015), <https://doi.org/10.1016/j.jallcom.2014.12.271>.
 - [16] P. Muthukumar, M. Prakash Maiya, S. Srinivasa Murthy, Performance tests on a thermally operated hydrogen compressor, *Int. J. Hydrogen Energy* (2008), <https://doi.org/10.1016/j.ijhydene.2007.07.019>.
 - [17] A. Witkowski, A. Rusin, M. Majkut, K. Stolecka, Comprehensive analysis of hydrogen compression and pipeline transportation from thermodynamics and safety aspects, *Energy* (2017), <https://doi.org/10.1016/j.energy.2017.05.141>.
 - [18] G. Karagiorgis, C.N. Christodoulou, H. von Storch, G. Tzamalīs, K. Deligiannis, D. Hadjipetrou, M. Odysseos, M. Roeb, C. Sattler, Design, development, construction and operation of a novel metal hydride compressor, *Int. J. Hydrogen Energy* (2017), <https://doi.org/10.1016/j.ijhydene.2017.03.195>.
 - [19] M. Lototsky, Y. Klochko, M.W. Davids, L. Pickering, D. Swanepoel, G. Louw, B. Van Der Westhuizen, S. Chidziva, C. Sita, B. Bladergroen, V. Linkov, Industrial-scale metal hydride hydrogen compressors developed at the South African Institute for Advanced Materials Chemistry, *Mater. Today Proc.* (2018), <https://doi.org/10.1016/j.matpr.2017.12.383>.
 - [20] N.A. Kelly, R. Girdwood, Evaluation of a thermally-driven metal-hydride-based hydrogen compressor, *Int. J. Hydrogen Energy* (2012), <https://doi.org/10.1016/j.ijhydene.2012.04.088>.
 - [21] M.V. Lototsky, V.A. Yartys, B.G. Pollet, R.C. Bowman, Metal hydride hydrogen compressors: a review, *Int. J. Hydrogen Energy* 39 (2014) 5818–5851. <https://doi.org/10.1016/j.ijhydene.2014.01.158>.
 - [22] E.I. Gkanas, 5 - metal hydrides: modeling of metal hydrides to be operated in a fuel cell, in: P. Ferreira-Aparicio, A.M. Chaparro (Eds.), *Portable Hydrog. Energy Syst.*, Academic Press, 2018, pp. 67–90. <https://doi.org/10.1016/B978-0-12-813128-2.00005-X>.
 - [23] R.C. Bowman, B. Fultz, Metallic hydrides I: hydrogen storage and other gas-phase applications, *MRS Bull.* 27 (2002) 688–693. <https://doi.org/10.1557/mrs2002.223>.
 - [24] R.C. Bowman, B. Fultz, Metallic hydrides I: hydrogen storage and other gas-phase applications, *MRS Bull.* 27 (2002) 688–693. <https://doi.org/10.1557/mrs2002.223>.
 - [25] G. Sandrock, State-of-the-art Review of Hydrogen Storage in Reversible Metal Hydrides for Military Fuel Cell Applications, 1997. ADA328073.
 - [26] G. Sandrock, A panoramic overview of hydrogen storage alloys from a gas reaction point of view, *J. Alloy. Comp.* 293–295 (1999) 877–888. [https://doi.org/10.1016/S0925-8388\(99\)00384-9](https://doi.org/10.1016/S0925-8388(99)00384-9).
 - [27] H. Uchida, Surface processes of H₂ on rare earth based hydrogen storage alloys with various surface modifications, *Int. J. Hydrogen Energy* 24 (1999) 861–869. [https://doi.org/10.1016/S0360-3199\(98\)00160-8](https://doi.org/10.1016/S0360-3199(98)00160-8).
 - [28] O.Y. Khyzhun, M.V. Lototsky, A.B. Riabov, C. Rosenkilde, V.A. Yartys, S. Jørgensen, R. V. Denys, Sn-containing (La,Mn)Ni₅-xSnxH₅-6 intermetallic hydrides: thermodynamic, structural and kinetic properties, *J. Alloy. Comp.* 356–357 (2003) 773–778. [https://doi.org/10.1016/S0925-8388\(03\)00352-9](https://doi.org/10.1016/S0925-8388(03)00352-9).
 - [29] R.C. Bowman Jr., C. Witham, B. Fultz, B.V. Ratnakumar, T.W. Ellis, I.E. Anderson, Hydrogen behavior of gas-atomized AB₅ alloys, *J. Alloy. Comp.* 253–254 (1997) 613–616. [https://doi.org/10.1016/S0925-8388\(96\)00299-5](https://doi.org/10.1016/S0925-8388(96)00299-5).
 - [30] V.K. Sharma, E. Anil Kumar, Thermodynamic analysis of two stage metal hydride based hydrogen compressor, *Mater. Today Proc.* 5 (2018) 23218–23223. <https://doi.org/10.1016/j.matpr.2018.11.053>.
 - [31] S. Luo, W. Luo, J.D. Clewley, T.B. Flanagan, R.C. Bowman, Thermodynamic and degradation studies of LaNi_{4.8}Sn_{0.2}-H₂ using isotherms and calorimetry, *J. Alloy. Comp.* 231 (1995) 473–478. [https://doi.org/10.1016/0925-8388\(95\)01870-0](https://doi.org/10.1016/0925-8388(95)01870-0).
 - [32] J.M. Park, J.Y. Lee, The intrinsic degradation phenomena of LaNi₅ and LaNi_{4.7}Al_{0.3} by temperature induced hydrogen absorption-desorption cycling, *Mater. Res. Bull.* (1987), [https://doi.org/10.1016/0025-5408\(87\)90255-8](https://doi.org/10.1016/0025-5408(87)90255-8).
 - [33] F. Yang, X. Cao, Z. Zhang, Z. Bao, Z. Wu, N.N. Serge, Assessment on the long term performance of a LaNi₅ based hydrogen storage system, *Energy Procedia* 29 (2012) 720–730. <https://doi.org/10.1016/j.egypro.2012.09.084>.
 - [34] R.C. Bowman, E.A. Payzant, P.R. Wilson, D.P. Pearson, A. Ledovskikh, D. Danilov, P.H.L. Notten, K. An, H.D. Skorpenske, D.L. Wood, Characterization and analyses of degradation and recovery of LaNi_{4.78}Sn_{0.22} hydrides following thermal aging, *J. Alloy. Comp.* 580 (2013) S207–S210. <https://doi.org/10.1016/j.jallcom.2013.03.129>.
 - [35] E.M. Borzone, M.V. Blanco, A. Baruj, G.O. Meyer, Stability of LaNi₅-xSnx cycled in hydrogen, *Int. J. Hydrogen Energy* 39 (2014) 8791–8796. <https://doi.org/10.1016/j.ijhydene.2013.12.031>.
 - [36] D.G. Ivey, D. Northwood, Storing hydrogen in AB₂ laves-type compounds, *Z. Phys. Chem.* 147 (1–2) (1986) 191–209. <https://doi.org/10.1524/zpch.1986.147.1.2.191>.
 - [37] D.G. Ivey, D.O. Northwood, Hydrogen storage characteristics of Zr(Bx₁B_{1-x}(\ extasciacutex)2B = Fe, Co,B(\ extasciacutex) = Cr, Mn, andx = 0.4, 0.5, 0.6, *J. Mater. Energy Syst.* 4 (1983) 222–228. <https://doi.org/10.1007/BF02833443>.
 - [38] L. Pickering, M.V. Lototsky, M. Wafeeq Davids, C. Sita, V. Linkov, Induction melted AB₂-type metal hydrides for hydrogen storage and compression applications, *Mater. Today Proc.* 5 (2018) 10470–10478. <https://doi.org/10.1016/j.matpr.2017.12.378>.
 - [39] W. Baumann, A. Leineweber, E.J. Mittemeijer, The kinetics of a polytypic Laves phase transformation in TiCr₂, *Intermetallics* 19 (2011) 526–535. <https://doi.org/10.1016/j.intermet.2010.11.027>.
 - [40] M. Williams, M.V. Lototsky, M.W. Davids, V. Linkov, V.A. Yartys, J.K. Solberg, Chemical surface modification for the improvement of the hydrogenation kinetics and poisoning resistance of TiFe, *J. Alloy. Comp.* 509 (2011) S770–S774. <https://doi.org/10.1016/j.jallcom.2010.11.063>.
 - [41] D. Planté, C. Raufast, S. Miraglia, P. de Rango, D. Fruchart, Improvement of hydrogen sorption properties of compounds based on Vanadium “bcc” alloys by mean of intergranular phase development, *J. Alloy. Comp.* 580 (2013) S192–S196. <https://doi.org/10.1016/j.jallcom.2013.03.080>.
 - [42] A. Kamble, P. Sharma, J. Huot, Effect of doping and particle size on hydrogen absorption properties of BCC solid solution 52Ti-12V-36Cr, *Int. J. Hydrogen Energy* 42 (2017) 11523–11527. <https://doi.org/10.1016/j.ijhydene.2017.02.137>.
 - [43] K. Goshome, N. Endo, M. Tetsuhiko, Evaluation of a BCC alloy as metal hydride compressor via 100 MPa-class high-pressure hydrogen apparatus, *Int. J. Hydrogen Energy* 44 (2019) 10800–10807. <https://doi.org/10.1016/j.ijhydene.2019.03.008>.
 - [44] T.A. Zotov, R.B. Sivov, E.A. Movlaev, S.V. Mitrokhin, V.N. Verbetsky, IMC hydrides with high hydrogen dissociation pressure, *J. Alloy. Comp.* 509 (2011) S839–S843. <https://doi.org/10.1016/j.jallcom.2011.01.198>.
 - [45] Bowman, et al., *International journal of research in physical chemistry and chemical physics*, *Z. Phys. Chem.* 181 (1993) 269–273.
 - [46] K.B. Minko, M.S. Bocharnikov, Y.B. Yanenko, M.V. Lototsky, A. Kolesnikov, B.P. Tarasov, Numerical and experimental study of heat-and-mass transfer processes in two-stage metal hydride hydrogen compressor, *Int. J. Hydrogen Energy* (2018), <https://doi.org/10.1016/j.ijhydene.2018.09.211>.
 - [47] B.G. Pollet, S. Pasupathi, G. Swart, K. Mouton, M. Lototsky, M. Williams, P. Bujlo, S. Ji, B.J. Bladergroen, V. Linkov, Hydrogen South Africa (HySA) systems competence centre: mission, objectives, technological achievements and breakthroughs, *Int. J. Hydrogen Energy* 39 (2014) 3577–3596. <https://doi.org/10.1016/j.ijhydene.2013.11.116>.
 - [48] F. Laurencelle, Z. Dehouche, J. Goyette, T.K. Bose, Integrated electrolyser—metal hydride compression system, *Int. J. Hydrogen Energy* 31 (2006) 762–768. <https://doi.org/10.1016/j.ijhydene.2005.06.019>.
 - [49] M. Lototsky, Y. Klochko, V. Linkov, P. Lawrie, B.G. Pollet, Thermally driven metal hydride hydrogen compressor for medium-scale applications, *Energy Procedia* 29 (2012) 347–356. <https://doi.org/10.1016/j.egypro.2012.09.041>.
 - [50] B.P. Tarasov, M.S. Bocharnikov, Y.B. Yanenko, P.V. Fursikov, M. V Lototsky, Cycling stability of RNi₅ (R = La, La+Ce) hydrides during the operation of metal hydride hydrogen compressor, *Int. J. Hydrogen Energy* 43 (2018) 4415–4427. <https://doi.org/10.1016/j.ijhydene.2018.01.086>.
 - [51] B. Satya Sekhar, S.P. Pailwan, P. Muthukumar, Studies on metal hydride based single-stage heat transformer, *Int. J. Hydrogen Energy* 38 (2013) 7178–7187. <https://doi.org/10.1016/j.ijhydene.2013.03.135>.
 - [52] P. Muthukumar, M. Prakash Maiya, S. Srinivasa Murthy, Experiments on a metal hydride based hydrogen compressor, *Int. J. Hydrogen Energy* 30 (2005) 879–892. <https://doi.org/10.1016/j.ijhydene.2004.09.003>.
 - [53] V.V. Solovey, A.I. Ivanovsky, V.I. Kolosov, Y.F. Shmal'ko, Series of metal hydride high pressure hydrogen compressors, *J. Alloy. Comp.* 231 (1995) 903–906. [https://doi.org/10.1016/0925-8388\(95\)01780-1](https://doi.org/10.1016/0925-8388(95)01780-1).
 - [54] M. Odysseos, P. De Rango, C.N. Christodoulou, E.K. Hlil, T. Steriotis, G. Karagiorgis, G. Charalamboulou, T. Papapanagiotou, A. Ampoumogli, V. Psycharis, E. Kouloukous, D. Fruchart, A. Stubos, The effect of compositional changes on the structural and hydrogen storage properties of (La–Ce)Ni₅ type intermetallics towards compounds suitable for metal hydride hydrogen compression, *J. Alloy. Comp.* 580 (2013) S268–S270. <https://doi.org/10.1016/j.jallcom.2013.01.057>.
 - [55] M.M.H. Bhuiya, C.Y. Lee, T. Hwang, S. Munira, R. Hopkins, H. Yoon, S.H. Park, K.J. Kim, Experimentally tuned dual stage hydrogen compressor for improved compression ratio, *Int. J. Hydrogen Energy* 39 (2014) 12924–12933. <https://doi.org/10.1016/j.ijhydene.2014.09.084>.

- doi.org/10.1016/j.ijhydene.2014.05.186.
- [56] Z. Dehouche, N. Grimard, F. Laurencelle, J. Goyette, T.K. Bose, Hydride alloys properties investigations for hydrogen sorption compressor, *J. Alloy. Comp.* 399 (2005) 224–236. <https://doi.org/10.1016/j.jallcom.2005.01.029>.
 - [57] X.H. Wang, Y.Y. Bei, X.C. Song, G.H. Fang, S.Q. Li, C.P. Chen, Q.D. Wang, Investigation on high-pressure metal hydride hydrogen compressors, *Int. J. Hydrogen Energy* 32 (2007) 4011–4015. <https://doi.org/10.1016/j.ijhydene.2007.03.002>.
 - [58] H. Li, X. Wang, Z. Dong, L. Xu, C. Chen, A study on 70MPa metal hydride hydrogen compressor, *J. Alloy. Comp.* 502 (2010) 503–507. <https://doi.org/10.1016/j.jallcom.2010.04.206>.
 - [59] E.D. Kouloukous, S.S. Makridis, E. Pavlidou, P. de Rango, A.K. Stubos, Investigation of ZrFe₂-type materials for metal hydride hydrogen compressor systems by substituting Fe with Cr or V, *Int. J. Hydrogen Energy* 39 (2014) 21380–21385. <https://doi.org/10.1016/j.ijhydene.2014.03.184>.
 - [60] L. Pickering, D. Reed, A.I. Bevan, D. Book, Ti–V–Mn based metal hydrides for hydrogen compression applications, *J. Alloy. Comp.* 645 (2015) S400–S403. <https://doi.org/10.1016/j.jallcom.2014.12.098>.
 - [61] P. Muthukumar, A. Kumar, N.N. Raju, K. Malleswararao, M.M. Rahman, A critical review on design aspects and developmental status of metal hydride based thermal machines, *Int. J. Hydrogen Energy* 43 (2018) 17753–17779. <https://doi.org/10.1016/j.ijhydene.2018.07.157>.
 - [62] S.S. Bhogilla, Design of a AB₂-metal hydride cylindrical tank for renewable energy storage, *J. Energy Storage* (2017), <https://doi.org/10.1016/j.est.2017.10.012>.
 - [63] X. Wang, H. Liu, H. Li, A 70 MPa hydrogen-compression system using metal hydrides, *Int. J. Hydrogen Energy* 36 (2011) 9079–9085. <https://doi.org/10.1016/j.ijhydene.2011.04.193>.
 - [64] E.I. Gkanas, D.M. Grant, M. Khzouz, A.D. Stuart, K. Manickam, G.S. Walker, Efficient hydrogen storage in up-scale metal hydride tanks as possible metal hydride compression agents equipped with aluminium extended surfaces, *Int. J. Hydrogen Energy* 41 (2016), <https://doi.org/10.1016/j.ijhydene.2016.04.035>.
 - [65] J.P. Vanhanen, M.T. Hagström, P.D. Lund, Combined hydrogen compressing and heat transforming through metal hydrides, *Int. J. Hydrogen Energy* 24 (1999) 441–448. [https://doi.org/10.1016/S0360-3199\(98\)00095-0](https://doi.org/10.1016/S0360-3199(98)00095-0).
 - [66] Ergenics Corp. <http://www.ergenics.com/compression.html>. (Accessed 25 April 2019).
 - [67] M. Lototsky, H. Halldors, Y. Klochko, J. Ren, V. Linkov, 7e200 bar/60 L/h continuously operated metal hydride hydrogen compressor, *Hydrogen materials science and chemistry of carbon nanomaterials/ICHMS*, 2009, p. 25e31.
 - [68] G. Popeneciu, V. Almasan, I. Coldea, D. Lupu, I. Misan, O. Ardelean, Investigation on a three-stage hydrogen thermal compressor based on metal hydrides, *J. Phys. Conf. Ser.* (2009), <https://doi.org/10.1088/1742-6596/182/1/012053>.
 - [69] J.-K. Kim, I.-S. Park, K.J. Kim, K. Gawlik, A hydrogen-compression system using porous metal hydride pellets of LaNi₅-xAl, *Int. J. Hydrogen Energy* 33 (2008) 870–877. <https://doi.org/10.1016/j.ijhydene.2007.10.027>.
 - [70] H. Li, X. Wang, Z. Dong, L. Xu, C. Chen, A study on 70MPa metal hydride hydrogen compressor, *J. Alloy. Comp.* 502 (2010) 503–507. <https://doi.org/10.1016/j.jallcom.2010.04.206>.
 - [71] X. Wang, H. Liu, H. Li, A 70 MPa hydrogen-compression system using metal hydrides, *Int. J. Hydrogen Energy* 36 (2011) 9079–9085. <https://doi.org/10.1016/j.ijhydene.2011.04.193>.
 - [72] P. Muthukumar, M.P. Maiya, S.S. Murthy, Performance tests on a thermally operated hydrogen compressor, *Int. J. Hydrogen Energy* 33 (2008) 463–469. <https://doi.org/10.1016/j.ijhydene.2007.07.019>.
 - [73] F. Laurencelle, Z. Dehouche, F. Morin, J. Goyette, Experimental study on a metal hydride based hydrogen compressor, *J. Alloy. Comp.* 475 (2009) 810–816. <https://doi.org/10.1016/j.jallcom.2008.08.007>.
 - [74] M. Lototsky, Y. Klochko, V. Linkov, P. Lawrie, B.G. Pollet, Thermally driven metal hydride hydrogen compressor for medium-scale applications, *Energy Procedia* 29 (2012) 347–356. <https://doi.org/10.1016/j.egypro.2012.09.041>.
 - [75] E.I. Gkanas, S.S. Makridis, A.K. Stubos, Modeling and Simulation for Absorption-Desorption Cyclic Process on a Three-Stage Metal Hydride Hydrogen Compressor, 2013, <https://doi.org/10.1016/B978-0-444-63234-0.50064-6>.
 - [76] B.J. Hardy, D.L. Anton, Hierarchical methodology for modeling hydrogen storage systems. Part I: scoping models, *Int. J. Hydrogen Energy* 34 (2009) 2269–2277. <https://doi.org/10.1016/j.ijhydene.2008.12.070>.
 - [77] E.I. Gkanas, M. Khzouz, G. Panagakos, T. Statheros, G. Mihalakakou, G.I. Siasos, G. Skodras, S.S. Makridis, Hydrogenation behavior in rectangular metal hydride tanks under effective heat management processes for green building applications, *Energy* (2018), <https://doi.org/10.1016/j.energy.2017.10.040>.
 - [78] A. Jemni, S.B. Nasrallah, Study of two-dimensional heat and mass transfer during absorption in a metal-hydrogen reactor, *Int. J. Hydrogen Energy* 20 (1995) 43–52. [https://doi.org/10.1016/0360-3199\(93\)E0007-8](https://doi.org/10.1016/0360-3199(93)E0007-8).
 - [79] T. Nakagawa, A. Inomata, H. Aoki, T. Miura, Numerical analysis of heat and mass transfer characteristics in the metal hydride bed, *Int. J. Hydrogen Energy* 25 (2000) 339–350. [https://doi.org/10.1016/S0360-3199\(99\)00036-1](https://doi.org/10.1016/S0360-3199(99)00036-1).
 - [80] F. Askari, A. Jemni, S. Ben Nasrallah, Study of two-dimensional and dynamic heat and mass transfer in a metal–hydrogen reactor, *Int. J. Hydrogen Energy* 28 (2003) 537–557. [https://doi.org/10.1016/S0360-3199\(02\)00141-6](https://doi.org/10.1016/S0360-3199(02)00141-6).
 - [81] E.S. Kikkindes, M.C. Georgiadis, A.K. Stubos, Dynamic modelling and optimization of hydrogen storage in metal hydride beds, *Energy* 31 (2006) 2428–2446. <https://doi.org/10.1016/j.energy.2005.10.036>.
 - [82] P. Muthukumar, U. Madhavakrishna, A. Dewan, Parametric studies on a metal hydride based hydrogen storage device, *Int. J. Hydrogen Energy* 32 (2007) 4988–4997. <https://doi.org/10.1016/j.ijhydene.2007.08.010>.
 - [83] A.R. Galvis E, F. Leardini, J.R. Ares, F. Cuevas, J.F. Fernandez, Simulation and design of a three-stage metal hydride hydrogen compressor based on experimental thermodynamic data, *Int. J. Hydrogen Energy* 43 (2018) 6666–6676. <https://doi.org/10.1016/j.ijhydene.2018.02.052>.
 - [84] E.I. Gkanas, D.M. Grant, A.D. Stuart, C.N. Eastwick, D. Book, S. Nayeibossadri, L. Pickering, G.S. Walker, Numerical study on a two-stage metal hydride hydrogen compression system, *J. Alloy. Comp.* 645 (2015), <https://doi.org/10.1016/j.jallcom.2015.03.123>.
 - [85] K.B. Minko, M.S. Bocharnikov, Y.B. Yanenko, M.V. Lototsky, A. Kolesnikov, B.P. Tarasov, Numerical and experimental study of heat-and-mass transfer processes in two-stage metal hydride hydrogen compressor, *Int. J. Hydrogen Energy* (2018), <https://doi.org/10.1016/j.ijhydene.2018.09.211>.
 - [86] P. Muthukumar, K.S. Patel, P. Sachan, N. Singhal, Computational study on metal hydride based three-stage hydrogen compressor, *Int. J. Hydrogen Energy* 37 (2012) 3797–3806. <https://doi.org/10.1016/j.ijhydene.2011.05.104>.
 - [87] P. Muthukumar, M. Prakash Maiya, S.S. Murthy, Parametric studies on a metal hydride based single stage hydrogen compressor, *Int. J. Hydrogen Energy* 27 (2002) 1083–1092. [https://doi.org/10.1016/S0360-3199\(02\)00005-8](https://doi.org/10.1016/S0360-3199(02)00005-8).
 - [88] A.R. Galvis E, F. Leardini, J. Bodega, J.R. Ares, J.F. Fernandez, Realistic simulation in a single stage hydrogen compressor based on AB₂ alloys, *Int. J. Hydrogen Energy* 41 (2016) 9780–9788. <https://doi.org/10.1016/j.ijhydene.2016.01.125>.
 - [89] J.-H. Cho, S.-S. Yu, M.-Y. Kim, S.-G. Kang, Y.-D. Lee, K.-Y. Ahn, H.-J. Ji, Dynamic modeling and simulation of hydrogen supply capacity from a metal hydride tank, *Int. J. Hydrogen Energy* 38 (2013) 8813–8828. <https://doi.org/10.1016/j.ijhydene.2013.02.142>.
 - [90] E.I. Gkanas, M. Khzouz, Numerical analysis of candidate materials for multi-stage metal hydride hydrogen compression processes, *Renew. Energy* 111 (2017), <https://doi.org/10.1016/j.renene.2017.04.037>.
 - [91] E. Tsotsas, H. Martin, Thermal conductivity of packed beds: a review, *Chem. Eng. Process: Process Intensification* 22 (1987) 19–37.
 - [92] M. Pons, P. Dantzer, Heat transfer in hydride packed beds. II. A new experimental technique and results on LaNi₅ powder, *Z. Phys. Chem.* 183 (Part_1_2) (1994) 213–223.
 - [93] S.S. Mohammadshahi, T. Gould, E.M. Gray, C.J. Webb, An improved model for metal-hydrogen storage tanks – Part 1: model development, *Int. J. Hydrogen Energy* 41 (2016) 3537–3550. <https://doi.org/10.1016/j.ijhydene.2015.12.050>.
 - [94] E.W. Lemmon, M.O. McLinden, M.L. Huber, REFPROP: reference fluid thermodynamic and transport properties, in: NIST Stand Reference Database, vol. 23, 2007, No 8.0.
 - [95] U. Mayer, M. Groll, W. Supper, Heat and mass transfer in metal hydride reaction beds: experimental and theoretical results, *J. Less Common Met.* 131 (1987) 235–244. [https://doi.org/10.1016/0022-5088\(87\)90523-6](https://doi.org/10.1016/0022-5088(87)90523-6).
 - [96] T. Nishizaki, K. Miyamoto, K. Yoshida, Coefficients of performance of hydride heat pumps, *J. Less Common. Met.* (1983), [https://doi.org/10.1016/0022-5088\(83\)90372-7](https://doi.org/10.1016/0022-5088(83)90372-7).